Renewable Energy and Power Quality Journal
https://repqj.com/index.php/repqj/index
RE&PQJ, Vol. 23, No. 5, 2025

Optimizing the Training Effect of Power Substation Personnel by Combining Multi-Scenario Fusion Method of AR and Neuromorphic Technology

Yanxiang Ran[1], Wen Zhao[2], Wei Li[2], Yongzhi Li[2,*]

[1]Operation and Maintenance Department of State Geid Lvliang Electric Power Supply Company, Lvliang, 033000, Shanxi Province, China
[2]Department of Technology Digitalization of State Geid Lvliang Electric Power Supply Company, Lvliang, 033000, Shanxi Province, China
[*]Corresponding author's email: Ryx9463L@hotmail.com

Abstract. In view of the problem that the current power substation personnel training lacks neuromorphic computing support on the existing AR (Augmented Reality) system, resulting in insufficient ability of personnel to operate substation equipment, this paper constructs a multi-scenario training intelligent teaching system that combines AR and neuromorphic technology. First, this paper constructs an AR interaction model based on SLAM (Simultaneous Localization and Mapping), realizes the precise superposition of equipment information through visual inertial odometer and three-dimensional modeling, and provides operation guidance for virtual-real integration. Secondly, this paper designs a behavior recognition module based on spiking neural network (SNN), uses the time coding mechanism to convert the trainee's action trajectory into a pulse sequence, and uses the LIF neuron structure for time series modeling to achieve real-time classification and feedback of the operation process. Furthermore, a multi-scenario knowledge transfer algorithm and adaptive generation mechanism are introduced, combined with meta-learning and GNN (Graph Neural Network), to improve the system's generalization ability and personalized adaptation efficiency between different fault tasks; finally, a virtual-reality collaborative decision-making model is established, and the organic integration of AR guidance information and neuromorphic feedback is realized through the state machine and event-driven mechanism to form a closed-loop intelligent teaching system. The results show that the method significantly improves the trainees' average operation accuracy and average task completion efficiency. The trainees' operation accuracy and task completion efficiency retention rates reached 91% and 93% respectively 8 weeks after training, which enhances the trainees' sense of immersion in training and their knowledge mastery. The AR system also has high real-time performance and stability (the positioning error is mainly concentrated in 3.5~4.0 mm; the rendering delay is mainly concentrated in 18~20 ms). The conclusion provides new ideas and technical support for the intelligent training of power substations.

Key words. Power substation training, Augmented reality, Neuromorphic technology, Multi-scenario fusion, Spiking neural network

1. Introduction

With the in-depth advancement of smart grid construction, power substations are the core nodes of the power transmission and distribution system, and the operation level of their operation and maintenance personnel is directly related to the safety and stability of power grid operation [1-3]. Due to problems such as lag, it is difficult to meet the increasingly complex equipment structure and emergency response needs [4-6]. In recent years, the development of emerging technologies such as augmented reality (AR) and neuromorphic computing has provided a new path for building intelligent and immersive training systems [7-9]. However, how to effectively integrate these technologies and achieve dynamic adaptation and personalized teaching in multiple scenarios is still a key issue that needs to be broken through in current research.

In the research of intelligent training systems for power substations, several teams have conducted relevant explorations from different angles. Mondragón Bernal I F [10] proposed a substation training system based on virtual reality; exploring and interacting with real models in the virtual world through games, Yang T [11] fully explore the traffic patterns of substation networks and use transfer learning to solve the problem of insufficient labeled samples of abnormal traffic in substations, proposed a new method for detecting abnormal traffic in the station-level communication network of smart substations based on deep transfer learning; Ou J [12] proposed a target detection model based on an improved fast regional convolutional neural network for automatic

detection of five types of electrical equipment in substations. Felinska E A [13] believed that AR-based remote illustration played a role in minimally invasive surgery through gaze guidance and can be used to improve training effects; Ke Y [14] proposed a substation safety construction operation perception and early warning technology based on multi-dimensional information fusion, which significantly improved the safety level and intelligent control level of substation construction operations.

Several research teams have conducted in-depth explorations on the issues of multi-scenario fusion and intelligent feedback in substation training. Song J [15] proposed an AR system based on SLAM, which is easy to access in a mobile environment and reduces the burden on researchers; Sadhu V [16] proposed a new architecture based on deep convolution and long short-term memory neural networks to detect and classify drone misoperations based on real-time sensor data, with an overall accuracy rate of more than 85%. Liu H [17] proposed a transfer learning automatic parameter sharing technology based on multi-objective optimization by utilizing a multi-population particle swarm optimizer. Zhao Y [18] explored how multimodal feedback mechanisms can significantly enhance the realism and intuitiveness of virtual interactions, making the experience more attractive and immersive. Li Y [19] found that the accuracy of the online learning behavior prediction model based on SNN was as high as 99.80%, and pointed out that the main learning behaviors that affect learning outcomes are students' academic performance and participation. Although the above studies have achieved results in their respective fields, there are still some problems such as insufficient technical integration and weak multi-scenario modeling capabilities.

In order to improve the operational standardization and knowledge mastery efficiency of power substation personnel, the operation guidance and real-time feedback of virtual-reality fusion are realized by constructing an AR interaction model based on SLAM and an SNN behavior recognition module; multi-scenario knowledge transfer algorithm and adaptive generation mechanism are designed to improve the system's adaptability to complex working conditions. This method improves the accuracy of operation guidance under virtual-reality fusion, and also enhances the time series modeling capability of misoperation identification. It realizes the state sharing and event-driven feedback between the AR end and the neuromorphic module, significantly improves the system's generalization ability and training adaptation efficiency in multiple scenarios, and provides a new technical path and practical paradigm support for intelligent training of power substations.

2. Algorithm Design

As shown in Figure 1, the power substation personnel training system includes five core modules: AR interaction model, neuromorphic behavior recognition module, multi-scenario adaptation module based on knowledge transfer, virtual-reality collaborative decision-making module and adaptive scenario generation module. These five modules work together to build an intelligent and immersive training system, which effectively improves the trainees' operation accuracy and emergency response efficiency.

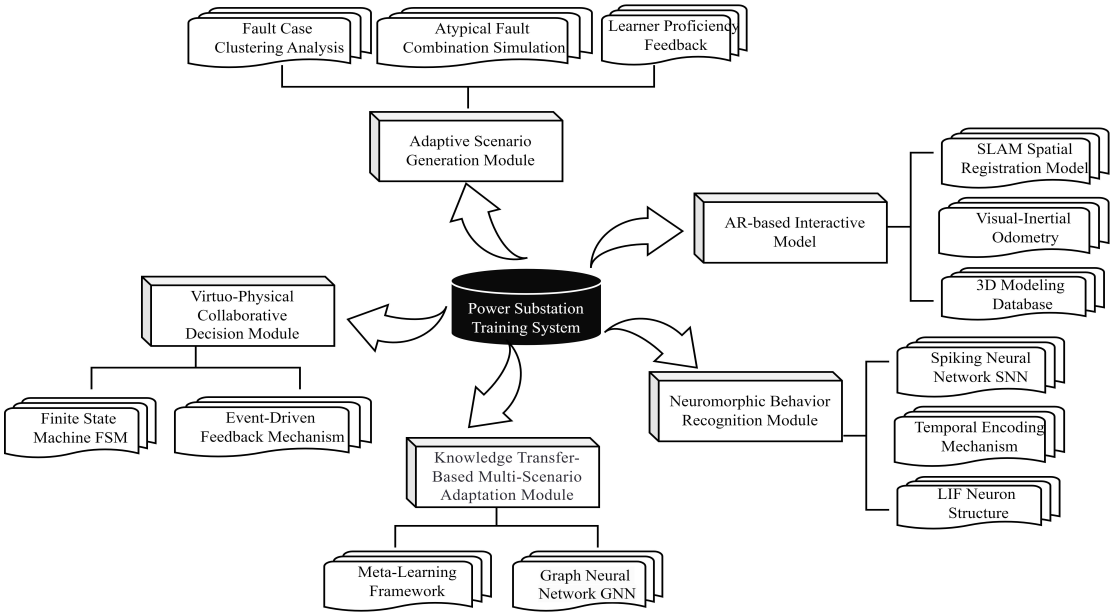

Figure 1. General diagram of the teaching system.

A. AR Interaction Model Construction

This paper constructs an AR spatial registration model based on SLAM (Simultaneous Localization and Mapping) [20]. This model uses visual-inertial odometry (VIO) technology to estimate the camera pose in real time in a mobile terminal or head-mounted display device, and accurately superimposes virtual operation guidance information on the physical environment in the form of 3D annotations [21,22]. Let the pose of the

camera at time t be $\mathbf{T}_t^w \in SE(3)$, which represents the transformation matrix from the world coordinate system w to the camera coordinate system c:

$$\mathbf{T}_t^w = \begin{bmatrix} \mathbf{R}_t^w & \mathbf{p}_t^w \\ \mathbf{0}^\top & \mathbf{1} \end{bmatrix} \quad (1)$$

$\mathbf{R}_t^w \in SO(3)$ represents the rotation matrix, and $\mathbf{p}_t^w \in \mathbb{R}^3$ represents the translation vector. The SLAM system is used to extract and match the key frame images to establish a sparse map point set $\mathcal{M} = \{\mathbf{m}_i \mid i = 1, \cdots, N\}$, where each map point $\mathbf{m}_i \in \mathbb{R}^3$ represents a three-dimensional feature point in the scene. The two-dimensional feature point $\mathbf{u}_j \in \mathbb{R}^2$ detected in the current frame image is associated with the three-dimensional map point through the projection equation:

$$u_j = \pi\left(\mathbf{T}_t^w \cdot m_i\right) \quad (2)$$

$\pi(\cdot)$ represents the perspective projection function, which is defined as follows:

$$\pi(\mathbf{X}) = \begin{bmatrix} f_x X/Z + c_x \\ f_y Y/Z + c_y \end{bmatrix} \quad (3)$$

f_x and f_y are the focal lengths of the camera, and $(c_x + c_y)$ is the coordinate of the main point of the image. On this basis, the IMU (Inertial Measurement Unit) sensor data is introduced, and the extended Kalman filter (EKF) is used to compensate for the visual positioning error. Assuming that the IMU measurement values are angular velocity and linear acceleration, its state update equation can be expressed as:

$$\mathbf{T}_t^w = f\left(\mathbf{T}_t^w, \mathbf{w}_t, \mathbf{a}_t\right) \quad (4)$$

Through the VIO fusion strategy, the robustness of the system is improved under complex working conditions such as lighting changes and occlusion, so that virtual information can maintain a stable and continuous registration effect in the physical space. A structured 3D model database is built for typical equipment in power substations (such as circuit breakers, disconnectors, and transformers). After completing the space registration, the system retrieves the corresponding 3D model $\mathcal{O}_k$ based on the device ID, and accurately superimposes it on the real scene through the model-image registration technology. Assuming that the model vertex set in the local coordinate system of the device is $\mathcal{V} = \{\mathbf{v}_l \mid l = 1, \cdots, M\}$, its projection in the camera coordinate system is:

$$v_l' = \mathbf{T}_o^{w^{-1}} \cdot \mathbf{T}_t^w \cdot \mathbf{v}_l \quad (5)$$

$\mathbf{T}_o^w$ is the position of the device in the world coordinate system, which is obtained by manual calibration before training. The transformed vertex $\mathbf{v}_l$ is projected onto the image plane to complete the rendering and superposition of the virtual operation guidance information, thereby realizing dynamic visualization support for the trainee's operation process.

B. Design of Neuromorphic Behavior Recognition Module

This paper constructs a behavior recognition model based on SNN [23-25]. The model uses a time encoding mechanism to convert the motion trajectory data collected by the inertial sensor into a time-series pulse signal, and simulates the dynamic response characteristics of the biological nervous system through a brain-like neuron structure to achieve high-precision motion classification and error detection. Suppose the input action is a three-dimensional acceleration sequence $\mathbf{a}(t) = \left[a_x(t), a_y(t), a_z(t)\right]^T \in \mathbb{R}^3$, where $t = 1, 2, \cdots, T$ represents the sampling time. In order to extract its time series features, it is first normalized:

$$\bar{a}(t) = \frac{a(t) - \mu_a}{\sigma_a} \quad (6)$$

μ_a and σ_a are the mean and standard deviation of the acceleration data in the training set. The time encoding strategy is used to convert the continuous signal into a pulse sequence. For each dimension $d \in \{x, y, z\}$, a threshold function $\theta_d(\cdot)$ is defined, and a pulse is triggered when the normalized acceleration value exceeds the threshold:

$$s_d(t) = \begin{cases} 1, & \text{if } \left|\bar{a}_d(t)\right| > \theta_d \\ 0, & \text{otherwise} \end{cases} \quad (7)$$

The final input pulse vector $\mathbf{s}(t) = \left[s_x(t), s_y(t), s_z(t)\right]^T$ is obtained as the first layer input of SNN. The SNN model adopts the Leaky Integrate-and-Fire (LIF) neuron structure, and its membrane potential dynamic evolution process is as follows:

$$\tau_m \frac{\mathrm{d}V_i(t)}{\mathrm{d}t} = -V_i(t) + R_m \sum_j w_{ij} s_j(t) \quad (8)$$

$V_i(t)$ is the membrane potential of the i-th neuron at time t; τ_m is the membrane time constant; R_m is the membrane resistance; w_{ij} is the connection weight from the j-th input neuron to the i-th neuron; $s_j(t)$ is whether the j-th input neuron emits a pulse at time t. When the membrane potential $V_i(t)$ exceeds the threshold V_{th}, the neuron emits a pulse and resets the

membrane potential:

$$V_i(t) \leftarrow \begin{cases} V_{\text{reset}}, & \text{if } V_i(t) \geq V_{\text{th}} \\ V_i(t), & \text{otherwise} \end{cases} \quad (9)$$

The entire SNN network is composed of multiple LIF layers stacked and trained through a supervised learning algorithm. This study uses an error back propagation approximation method based on spike-timing-dependent plasticity (STDP) to minimize the cross entropy loss function between the predicted label and the true action category:

$$\mathcal{L} = -\sum_{k=1}^{K} y_k \log \hat{y}_k \quad (10)$$

y_k is the true label of the sample (one-hot representation); $\hat{y}_k$ is the activation probability of the k th neuron in the SNN output layer.

By introducing the sliding time window mechanism, the system can analyze the continuous operation process in real time and complete a complete reasoning and feedback within $\Delta t = 200\text{ms}$, meeting the needs of rapid correction of misoperation in power substation training.

C. Design of Multi-Scenario Knowledge Transfer Algorithm

This paper proposes a multi-scenario knowledge transfer strategy based on the combination of meta-learning and graph neural network (GNN) [26-28]. This method aims to solve the model adaptation problem caused by the task differences between different fault types, so that the system can quickly adjust parameters when facing new tasks with only a small number of samples, thus achieving efficient training and personalized teaching. Let the task set $\mathcal{T} = \mathcal{T}_1, \mathcal{T}_2, \cdots, \mathcal{T}_N$ represent all possible fault operation tasks, each task $\mathcal{T}_i$ corresponds to a set of input-output sample pairs $\mathcal{D}_i = \left\{\left(\mathbf{x}_{ij}, y_{ij}\right)\right\}_{j=1}^{M_i}$, $\mathbf{x}_{ij} \in \mathbb{R}^d$ represents the student operation feature vector, and $y_{ij} \in \{1, \cdots, K\}$ represents the action category label. This study uses the MAML (Model-Agnostic Meta-Learning) framework for meta-training, with the goal of learning an initial parameter θ so that the model can quickly adapt to new tasks after a small amount of gradient updates on any task $\mathcal{T}_i$. In each meta-training iteration, a task $\mathcal{T}_i$ is sampled from the task distribution $p(\mathcal{T})$ and its training set D_i^{tr} is used to update the model parameters:

$$\theta_{i'} = \theta - \alpha \nabla_\theta L_{J_i}(\theta) \quad (11)$$

$\mathcal{L}_{J_i}(\cdot)$ is the loss function of task J_i , α is the inner layer learning rate. The meta-gradient is calculated using the validation set $\mathcal{D}_i^{\text{val}}$ of task J_i , and the initial parameter θ is updated:

$$\nabla_\theta \mathcal{L}_{\text{meta}} = \nabla_\theta \mathcal{L}_{\mathcal{T}_i}\left(\theta_i'\right) = \nabla_{\theta_i'} \mathcal{L}_{\mathcal{T}_i}\left(\theta_i'\right) \cdot \nabla_\theta \theta_i' \quad (12)$$

$$\theta \leftarrow \theta - \beta \nabla_\theta \mathcal{L}_{\text{meta}} \quad (13)$$

β is the outer learning rate. In order to further explore the semantic relationship between tasks, GNN is introduced to construct the task dependency graph $\mathcal{G} = (\mathcal{V}, \mathcal{E})$. The node set $\mathcal{V}$ represents each task $\mathcal{T}_i$, and the edge set $\mathcal{E}$ represents the similarity or causal relationship between tasks. The adjacency matrix $A \in \{0,1\}^{N \times N}$ is defined. If tasks $\mathcal{T}_i$ and $\mathcal{T}_j$ have similar operation processes or share some equipment, then $A_{ij} = 1$, otherwise it is 0. The task representation is aggregated and abstracted through the graph convolutional network (GCN):

$$H^{(l+1)} = \sigma\left(\bar{D}^{-\frac{1}{2}} \bar{A} \bar{D}^{-\frac{1}{2}} H^{(l)} W^{(l)}\right) \quad (14)$$

$H^{(l)} \in \mathbb{R}^{N \times d_l}$ is the node embedding of the l layer; $\bar{A} = A + I_N$ is the adjacency matrix with self-loops added; $\bar{D}$ is the corresponding degree matrix; $W^{(l)}$ is the learnable parameter; $\sigma(\cdot)$ is the activation function. The task representation $h_i \in \mathbb{R}^{d'}$ extracted by GNN is introduced into the meta-learning framework as the auxiliary parameter initialization of the task context information:

$$\theta_i' = \theta(h_i) - \alpha \nabla_{\theta(h_i)} \mathcal{L}_{\mathcal{T}_i}\left(\theta(h_i)\right) \quad (15)$$

Through this mechanism, the system can quickly adapt to an unprecedented combination of faults based on the knowledge of existing tasks, significantly improving the generalization ability and training efficiency in multiple scenarios.

Figure 2 shows the multi-task knowledge transfer and adaptive generation process combining meta-learning (MAML) and GCN. First, a set of tasks are selected from the task set sampling for training, the model parameters are initialized through the MAML meta-learning framework, and the inner loop update is performed on each task to quickly adapt to new tasks. Next, the validation set is used to evaluate the model performance and update the external parameters. At the same time, the adjacency matrix A is constructed based on the similarity and causal relationship between tasks, and the task representation is encoded through the GCN to achieve adaptive learning of task embedding. Finally, the system outputs adaptive strategies for new tasks, including rapid adaptation capabilities and generalization capabilities for

unseen tasks. The entire process aims to improve the versatility and personalized adaptability of the model in multiple scenarios, thereby improving the overall performance and teaching effect of the system.

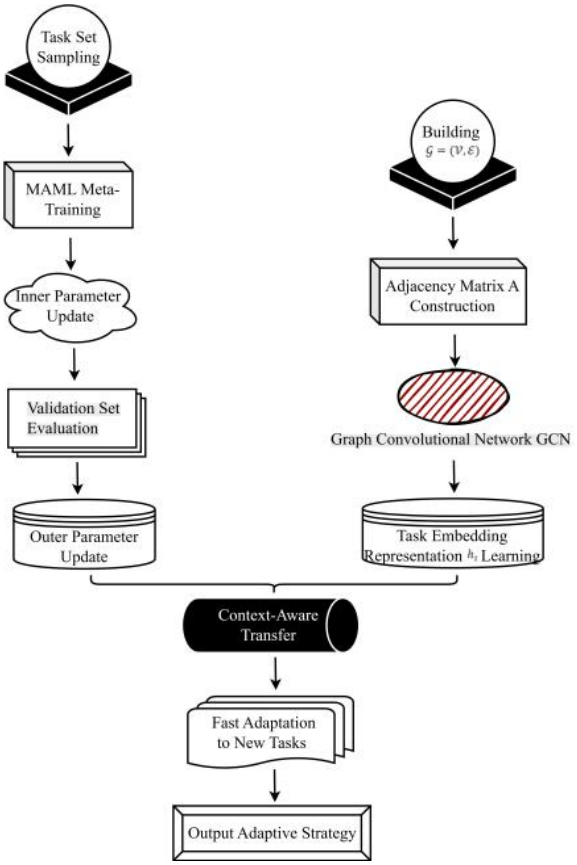

Figure 2. Knowledge transfer process.

D. Modeling of Virtual-Real Collaborative Decision-Making Mechanism

In order to realize the organic integration of AR guidance information and neuromorphic behavior recognition results in the training process of power substation personnel, this paper constructs a virtual-reality collaborative decision-making model based on state machine and event-driven [29]. This model realizes real-time judgment and response control of trainees' operation behaviors through shared state variables and dynamic feedback mechanism, forming a closed-loop intelligent teaching system. Assume that the state space of the system is $\mathcal{S}=\{s_1,s_2,\cdots,s_N\}$, and each state s_i represents a key node in the current operation process, such as "device identification completed", "operation path loading", "misoperation warning triggered", etc. During the operation of the system, the state transition is jointly determined by the current operation context $o_t \in \mathcal{O}$ and the behavior evaluation value $a_t \in \mathcal{A}$ output by the neuromorphic module:

$$s_{t+1} = f(s_t, o_t, a_t) \quad (16)$$

$f(\cdot)$ is the state transfer function; o_t is the operating environment context information perceived by the AR end; a_t is the action classification label or risk score output by the neuromorphic module. The neuromorphic module uses SNN for action recognition and outputs a confidence vector $\mathbf{p}_t = \left[p_1^{(t)}, p_2^{(t)}, \cdots, p_K^{(t)}\right]^T \in [0,1]^K$, which represents the probability distribution of t for K-type operation actions at the moment. If the category corresponding to the highest probability is an abnormal operation (such as accidentally touching a non-target device), a high-priority feedback event is triggered:

$$e_t = \begin{cases} 1, & \arg\cdot\max_k \cdot\, p_k^{(t)} = \text{anomaly} \\ 0, & \text{otherwise} \end{cases} \quad (17)$$

The AR end dynamically adjusts the guidance strategy based on the current state s_t and event flag e_t. Define the guidance information set $\mathcal{G}=\{g_1,g_2,\cdots,g_M\}$, where each element g_M represents a type of visual prompt (such as 3D annotation, arrow guidance, color flashing, etc.). The final displayed guidance instruction $g_t \in \mathcal{G}$ is generated by the following mapping:

$$g_t = h(s_t, e_t) \quad (18)$$

$h(\cdot)$ is a preset decision rule function, which can be expressed as a finite state machine (FSM), as shown in Table 1.

Table 1. Finite State Machine.

Current State s_t	Input Condition e_t	Next State s_{t+1}	Output Action g_t
Normal Operation	0	Normal Operation	Continue path guidance
Normal Operation	1	Anomaly Warning	Display error alert & correction suggestion
Anomaly Warning	0	Recovery	Provide subsequent step instructions
Anomaly Warning	1	Continuous Alert	Enhance visual warning & pause workflow

In order to improve the real-time and stability of system response, an event-driven timestamp synchronization mechanism is introduced:

$$\Delta t = \left\| t_{\text{AR}} - t_{\text{SNN}} \right\| < \tau \quad (19)$$

t_{AR} and t_{SNN} represent the latest update timestamps of the AR module and the neuromorphic module, respectively, and τ is the maximum allowed time difference threshold (set to 200ms). When the two are out of sync, the system can give priority to the most

recent valid recognition result for feedback to ensure teaching continuity.

E. Scenario Adaptive Generation Mechanism

In order to improve the diversity and personalized adaptation capabilities of the power substation personnel training system, this paper proposes a multi-dimensional scenario adaptive generation mechanism based on historical training data and expert experience [30]. This mechanism dynamically adjusts the training scenario through fault case clustering analysis, atypical fault combination simulation and trainee mastery status feedback to meet the learning needs of trainees at different levels. Assume that the historical fault operation records constitute a sample set:

$$\mathcal{D}=\left\{\left(\mathbf{x}_1,y_1\right),\left(\mathbf{x}_2,y_2\right),\cdots,\left(\mathbf{x}_N,y_N\right)\right\} \quad (20)$$

$\mathbf{x}_i\in\mathbb{R}^d$: The operation feature vector of the i -th sample, including equipment type, operation sequence, action timing, etc.; $y_i\in\{1,2,\cdots,K\}$ corresponds to the fault category label (such as circuit breaker abnormality, instrument misreading, grounding failure, etc.). An unsupervised clustering method is used to classify existing fault cases and extract typical working condition characteristics. Define the cluster center set:

$$\mathcal{C}=\left\{\mathbf{c}_1,\mathbf{c}_1,\cdots,\mathbf{c}_K\right\},\mathbf{c}_k\in\mathbb{R}^d \quad (21)$$

Use the K -Means algorithm to minimize the following objective function:

$$J=\sum_{k=1}^{K}\sum_{\mathbf{x}_i\in\mathcal{G}_k}\left\|\mathbf{x}_i-\mathbf{c}_k\right\|^2 \quad (22)$$

$\mathcal{G}_k$ represents the sample set assigned to the k th cluster. After obtaining the typical fault mode, the mutation operator is further introduced to simulate atypical or compound fault combinations to enhance training diversity. The mutation operation function $\Psi(\cdot)$ is defined, which is used to impose a small perturbation on the original sample $\mathbf{x}_i$ and change some operation properties:

$$\mathbf{x}_i'=\Psi\left(\mathbf{x}_i\right)=\mathbf{x}_i+\varepsilon\cdot\delta \quad (23)$$

ε is a hyperparameter that controls the intensity of disturbance; $\delta\in\{-1,0,1\}^d$ represents the direction of change in the operation attributes of each dimension. A scenario complexity adjustment module can be constructed to dynamically adjust the difficulty of the generated scenario according to the student's current mastery level. Assume that the student's knowledge mastery level is represented by the probability distribution output by the evaluation model:

$$\mathbf{p}_t=\left[p_1^{(t)},p_2^{(t)},\cdots,p_K^{(t)}\right]^T\in[0,1]^K \quad (24)$$

$p_k^{(t)}$ represents the probability that the trainee can master the kth type of fault at time t. Define the scenario difficulty factor $\eta_t\in[0,1]$ to control the proportion of high-risk operations in the newly generated scenario:

$$\eta_t=\alpha\cdot\left(1-\max_k p_k^{(t)}\right)+(1-\alpha)\cdot\frac{1}{K}\sum_{k=1}^{K}\left(1-p_k^{(t)}\right) \quad (25)$$

$\alpha\in[0,1]$ is the balance coefficient, which reflects the weight of individual differences and overall performance. The scene generation process is modeled as a Markov decision process (MDP) and optimized through deep reinforcement learning strategy. Define the five-tuple:

$$\mathcal{M}=(\mathcal{S},\mathcal{A},\mathcal{T},\mathcal{R},\gamma) \quad (26)$$

$\mathcal{S}$ is the state space, which represents the current task characteristics and the trainee's mastery status; $\mathcal{A}$ is the action space, which represents the optional fault combinations and operation sequences; $\mathcal{T}$ is the state transfer function; $\mathcal{R}$ is the reward function, which is defined as $r_t=w_1\cdot\text{TaskSuccessRate}+w_2\cdot\text{ErrorDiscoveryCount}$. w_1 and w_2 are weight coefficients, which measure the importance of task completion quality and error recognition ability respectively; $\gamma\in[0,1]$ represents the discount factor. The policy function is modeled using the Deep Q-Network (DQN) to maximize the long-term return expectation:

$$\pi^*=\arg\max_{\pi}\mathbb{E}\left[\sum_{t=0}^{T}\gamma^t r_t\right] \quad (27)$$

Through the above mechanism, the system can support the free combination of no less than 10 typical fault types, and dynamically adjust the complexity of the training scenario according to the real-time performance of the trainees to achieve personalized and progressive teaching goals.

3. Experiment and Verification

A. Experimental Design

A simulation training platform including typical power substation equipment (circuit breakers, disconnectors, grounding devices, etc.) was built to support AR visualization guidance (accurate early warning of virtual information and physical environment through SLAM technology), SNN behavior recognition feedback (real-time modeling and feedback of fixture operation behavior based on SNN), and multi-scenario automatic generation (dynamically generate failure scenarios of varying complexity based on historical load performance and mission requirements) functions. The platform is

built based on the combination of physical entities and virtual modeling, and mainly includes the following components: physical training environment, three-dimensional digital model library construction, augmented reality interaction system, behavior recognition and feedback module, multi-scenario generation mechanism, and data collection and evaluation system.A total of 30 trainees with primary operation and maintenance experience were recruited to participate in the experiment. Participants were required to have at least six months of substation operation or maintenance experience; be between 30 and 40 years old to ensure physical ability and minimize age-related cognitive changes; have no known visual impairment, motor impairment, or other conditions that would impede their ability to use AR devices or perform physical tasks; and be proficient in Mandarin to ensure comprehension of the training materials and questionnaires. To ensure fairness and reduce selection bias, the 30 participants were randomly assigned to two groups using a computer-generated random number list. The control group adopted the traditional desktop teaching + video explanation method, and the experimental group used the intelligent training system that integrates AR and neuromorphic technology proposed in this paper for training. All trainees need to complete two types of tasks: standard operating procedure tasks (complete the operating steps of the specified equipment according to the specifications) and emergency fault handling drills (quickly locate the problem and take correct measures in the event of an emergency fault). Data is collected through system logs and questionnaires, and comparative analysis is performed. Central Processing Unit (CPU): Intel Core i7-13700K; Graphics Processing Unit (GPU): RTX 3060.

B. Evaluation of Trainee Operation Accuracy

The SNN behavior recognition module is used to determine the trainee's action category in real time, and combined with the preset procedure database to determine whether the action meets the specifications. The operation accuracy is defined as:

$$\text{Accuracy} = \frac{\text{Correct Actions}}{\text{Total Actions}} \times 100\% \quad (28)$$

The number of key operation steps and errors of each student in multiple training rounds was recorded, and the accuracy index was calculated. The experimental group was automatically identified and prompted for incorrect operations by the system, while the control group was manually scored and counted by experts.

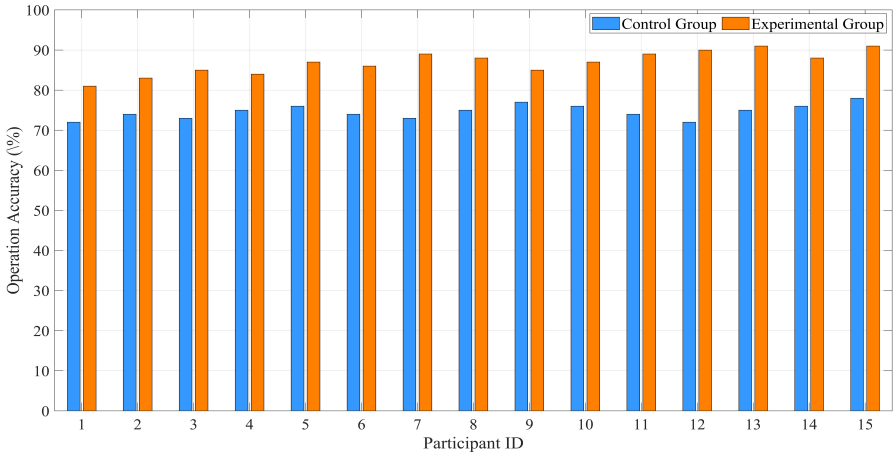

Figure 3. Comparison of operation accuracy.

Figure 3 shows the comparison of the operation accuracy of the control group and the experimental group. The X-axis is the 15 numbers and the Y-axis is the corresponding operation accuracy (%). The accuracy of the control group students ranged from 72% to 78%, with a small overall fluctuation, indicating that the traditional training method provided limited guidance on standardized operations for students and it was difficult to form a significant difference. The accuracy of the experimental group was significantly improved, ranging from 81% to 91%. Among them, students No. 13 and No. 15 even reached 91%, indicating that the teaching system integrating AR and neuromorphic technology effectively improved the standardization level of students' operations. The comparison shows that the accuracy rate of each trainee in the experimental group is higher than that in the control group, reflecting the universal applicability of this method in terms of training effect.

The system uses SLAM to achieve accurate superposition of device information and physical environment, allowing trainees to obtain real-time visual guidance in the AR interface and reduce the occurrence of misoperation. The SNN-based behavior recognition model can model the trainees' actions in time series, combine the action trajectory data collected by the inertial sensor, classify and identify the key steps in the operation process, and provide immediate feedback and correction suggestions when errors are detected. The existence of this closed-loop teaching mechanism has enabled the trainees in the experimental group to form more standardized operating habits after multiple trainings, and the accuracy rate is significantly higher than the traditional training method using manual scoring, which shows that the method has good application potential and teaching value in the training of power substation personnel.

C. *Emergency Response Efficiency Evaluation*

Two emergency failure scenarios can be set to record the total time taken by trainees from the occurrence of the failure to the completion of the processing, in seconds (s), to measure emergency response capabilities. The average response time is defined as:

$$\bar{T}_{\text{response}} = \frac{1}{N}\sum_{i=1}^{N} T_i^{\text{response}} \quad (29)$$

T_i^{response} represents the response time of the i th student, and N is the sample size.

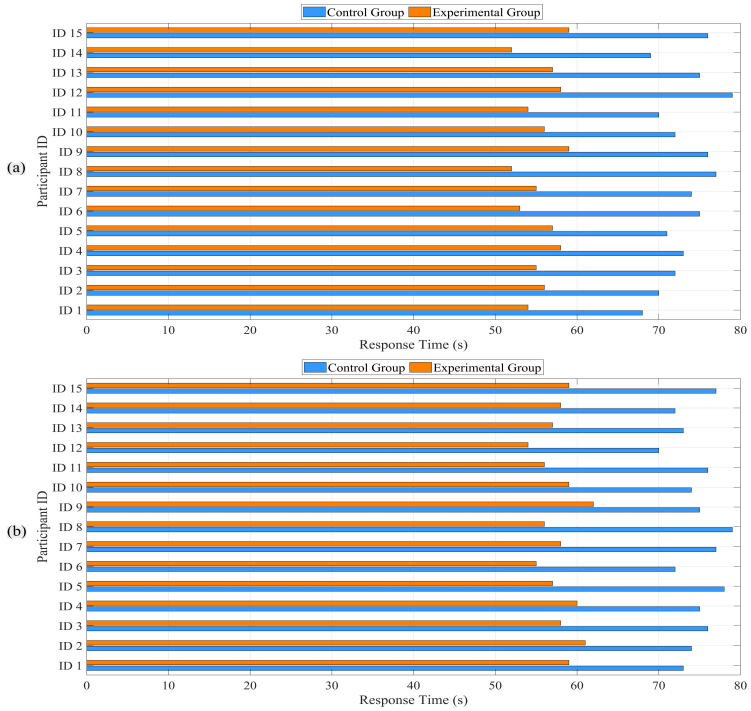

Figure 4. Emergency response efficiency evaluation. Figure 4 (a) Sudden failure scenario 1; Figure 4 (b) Sudden failure scenario 2.

Figures 4 (a) and (b) show the comparison of the students' operation response time in the control group and the experimental group under sudden failure scenarios 1 and 2, respectively. From the overall data, the response time of the experimental group in both scenarios is generally lower than that of the control group. In the sudden failure scenario 1, the response time of the control group was distributed between 68 and 79 seconds, while that of the experimental group was concentrated between 52 and 59 seconds. In scenario 2, the response time of the control group was mostly in the range of 70 to 79 seconds, while that of the experimental group was stable in the range of 54 to 62 seconds. Whether in scenario 1 or 2, the experimental group showed faster and more consistent response performance, reflecting that the proposed teaching system integrating AR and neuromorphic technology has obvious advantages in improving students' emergency response capabilities.

The system provides clear operation process prompts through AR operation guidance built by SLAM, enabling trainees to locate equipment more quickly and perform correct actions; the SNN module performs temporal modeling of trainee behavior, identifies misoperations in real time and provides feedback on correction suggestions, effectively reducing judgment delays and error correction time. In the sudden failure scenario 1, the average response time of the trainees dropped from 73 seconds in the control group to 56 seconds in the experimental group. In scenario 2, the average response time also dropped from 75 seconds to 58 seconds, reflecting the system's good adaptability and teaching closed-loop control capabilities under complex working conditions. The standard deviation of the experimental group's response time in both scenarios was small, indicating that the system training effect had high consistency and stability. This further verifies the effective role of this method in enhancing emergency response capabilities in power substation personnel training.

D. *Scenario Adaptability Evaluation*

Five different types of fault task scenarios were set, including short-circuit tripping, instrument abnormality, erroneous operation recovery and other complex working conditions. The completion rate of trainees in each type of task was calculated, that is, the proportion of trainees who successfully completed the task. The formula is:

$$\text{Completion Rate}_k = \frac{\text{Number of Successful Attempts in Scenario } k}{\text{Total Number of Attempts in Scenario } k} \quad (30)$$

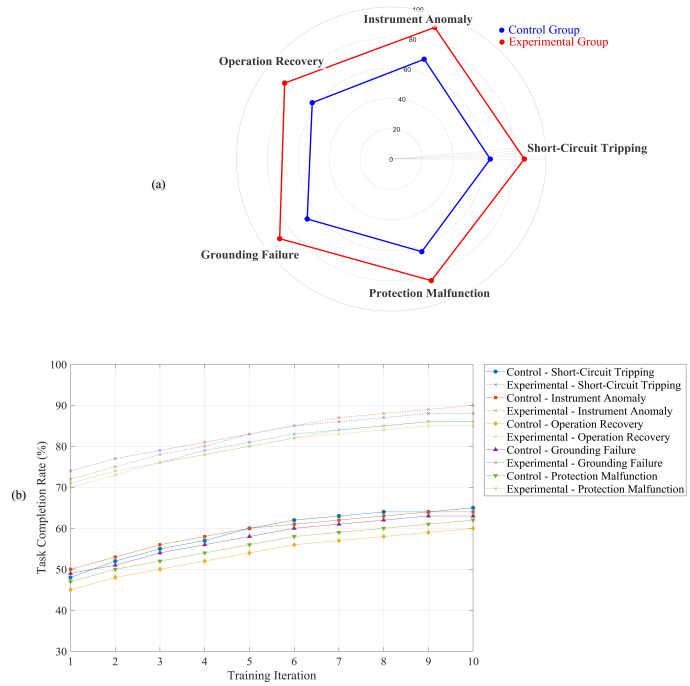

Figure 5. Scenario adaptability evaluation. Figure 5 (a) Task completion rate; Figure 5 (b) Completion rate change trend of 10 rounds of training.

Figure 5 shows the average task completion rate and completion rate change trend of the control group and the experimental group under five typical fault scenarios. Figure 5 (a) is a radar chart, including short-circuit tripping, instrument abnormality, erroneous operation recovery, grounding failure and protection malfunction. Each angle direction represents a specific scene. The average values of the control group in the five scenes are concentrated in 63%~69%, while the experimental group generally reaches 84%~91%, showing a significantly higher contour area and overall performance. Figure 5 (b) further shows the changing trend of the trainees' task completion rate in 10 rounds of training, with the X-axis representing the training round and the Y-axis representing the completion rate (%). The control group improved slowly and had a low final completion rate, such as short-circuit tripping, which ultimately reached only 65%, while the experimental group showed a high initial completion rate in the early stages and stabilized in the later stages. For example, in the instrument abnormality scenario, the completion rate of the experimental group reached 90% in the 10th round, which intuitively reflected the significant advantages of the experimental group in multi-scenario adaptability.

The completion rate of the experimental group in each scene in Figure 5 (a) is higher than that of the control group. The improvement is obvious in tasks that rely on judgment and feedback mechanisms, such as "instrument abnormality" and "grounding failure", reaching 91% and 89% respectively, indicating that the SNN behavior recognition module can effectively capture the timing characteristics of actions and provide timely correction prompts. The experimental group in Figure 5 (b) was able to quickly understand the task logic in the early stages, thanks to the closed-loop teaching mechanism formed by the AR visualization guidance built by SLAM and the real-time feedback driven by SNN. This virtual-real collaborative approach improves learning efficiency and enables trainees to have stronger migration capabilities between different scenarios, maintaining a stable high-level performance in a variety of fault tasks, reflecting the effectiveness and practicality of this method in intelligent training of power substations.

E. Subjective Rating of Training Immersion

This paper uses the Likert five-level scale to score the quality of AR experience, covering five dimensions: interface friendliness, guidance clarity, environmental realism, feedback timeliness, and overall satisfaction. Each trainee fills out a questionnaire after each training to form subjective rating data. Table 2 summarizes the mean scores of each dimension.

Table 2. Subjective rating of training immersion.

Dimension	Control Group (Max=5)	Experimental Group (Max=5)
Interface Friendliness	3.1	4.6
Guidance Clarity	3	4.7
Environmental Realism	3.2	4.8
Feedback Timeliness	3.3	4.9
Overall Satisfaction	3.2	4.7

Table 2 shows the average scores of the control group and the experimental group on the five dimensions of training immersion, which were evaluated using a five-point Likert scale with a full score of 5 points, covering interface friendliness, guidance clarity, environmental realism, feedback timeliness, and overall satisfaction. From the data, the scores of the control group in various dimensions are generally concentrated between 3.0 and 3.3, reflecting that the traditional training method has obvious deficiencies in interactive experience and immersion. The scores of the experimental group have significantly improved, among which the timely feedback has reached 4.9 points, the environmental realism has reached 4.8 points, and the clarity of guidance and overall satisfaction have both reached 4.7 points. This shows that the trainees have a high degree of recognition of the teaching system that integrates AR and neuromorphic technology in terms of visual guidance, real-time feedback and operational immersion. By comparison, it can be seen that the experimental group outperformed the control group in all dimensions, especially in "timely feedback" and "environmental realism", which reflects the advantages of the system in virtual-real fusion teaching.

The SLAM-based AR system realizes the precise superposition of equipment information and physical environment, enabling students to complete operation tasks in a virtual environment with a strong sense of reality, thereby improving the subjective scores of "environmental realism" and "guidance clarity". The SNN module has good time coding capabilities and pushes correction prompts immediately when it detects a tendency for misoperation. This is directly reflected in the "timely feedback" score of 4.9, which is much higher than the 3.3 points of the control group. The closed-loop feedback mechanism of the system enhances the trainees' trust and participation in the training process, and ultimately makes the "overall satisfaction" score reach 4.7 points. This intelligent teaching design based on virtual-real collaboration not only improves the students' operating experience, but also provides solid technical support for personalized training. It is an important foundation for realizing a highly immersive and highly adaptable power substation training system.

F. Knowledge Mastery Assessment

A standardized question bank is used to conduct pre-tests and post-tests on students, covering equipment principles, operating procedures, fault judgment, etc. The knowledge mastery improvement is defined as:

$$\Delta S = S_{\text{post}} - S_{\text{pre}} \quad (31)$$

S_{pre} is the pre-test score, and S_{post} is the post-test score. Figure 5 is a line graph comparing the pre- and post-test scores.

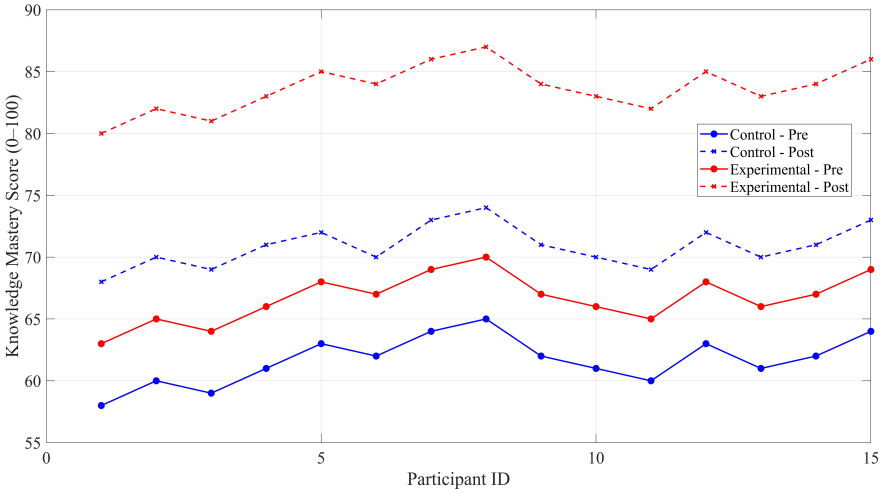

Figure 6. Knowledge mastery assessment.

Figure 6 shows the changing trend of knowledge mastery of the control group and the experimental group before and after training. The X-axis is the number of the 15 trainees, and the Y-axis is the assessment score (full score 100 points). From the data, the average score of the experimental group after training is significantly higher than that of the control group. For example, the post-test score of ID 8 in the experimental group reached 87 points, while its pre-test score was only 71 points, an increase of 16 points. Compared with the control group, the score of ID 8 increased from 65 points to 74 points, an increase of only 9 points. Overall, the improvement of the experimental group students is generally between 15 and 19 points, while the control group is mostly concentrated in the range of 6 to 10 points, reflecting the problem of slow knowledge absorption under the traditional teaching method. The chart intuitively reflects the superiority of the teaching system integrating AR and neuromorphic technology in promoting knowledge mastery through clear line comparison.

The fundamental reason for the significant improvement in the knowledge mastery of the experimental group lies in the virtual-reality fusion teaching mechanism proposed in this paper. The AR interactive model based on SLAM can provide three-dimensional visual

operation guidance, allowing students to understand the equipment structure and operation process more intuitively. The SNN behavior recognition module dynamically models the students' answering process, provides real-time feedback on the knowledge points, and guides them to correct their misconceptions. This closed-loop teaching strategy effectively improves students' learning efficiency and memory retention ability. Most students in the experimental group scored more than 80 points after training, indicating that the system has improved basic cognitive levels and enhanced the ability to understand and apply complex knowledge points. The multi-scenario adaptive generation mechanism enables each student to receive personalized training on different knowledge points, thus avoiding the learning bottleneck caused by "unified teaching + unified testing". These advantages have contributed to the significant improvement of the experimental group's pre- and post-test scores, verifying the effectiveness of the proposed method in improving knowledge mastery.

G. AR System Performance Evaluation

The real space coordinates are collected as a reference benchmark through high-precision calibration equipment, and the Euclidean distance difference between the system output posture and the true value is calculated as the positioning error. The specific formula is as follows:

$$\text{Localization Error} = \sqrt{(x_{\text{est}} - x_{\text{true}})^2 + (y_{\text{est}} - y_{\text{true}})^2 + (z_{\text{est}} - z_{\text{true}})^2} \quad (32)$$

x_{est} , y_{est} , and z_{est} represent the estimated position coordinates of the system, and x_{true} , y_{true} and z_{true} represent the real coordinate values obtained by the calibration device. At the same time, a timestamp mark is inserted in the key path from image acquisition to screen rendering completion, and the time difference between the two is calculated to obtain the single-frame rendering delay. The formula is:

$$\text{Rendering Latency} = t_{\text{render}} - t_{\text{capture}} \quad (33)$$

t_{render} is the rendering completion time, and t_{capture} is the image acquisition start time. This indicator reflects the real-time response of the system in the virtual-real fusion process.

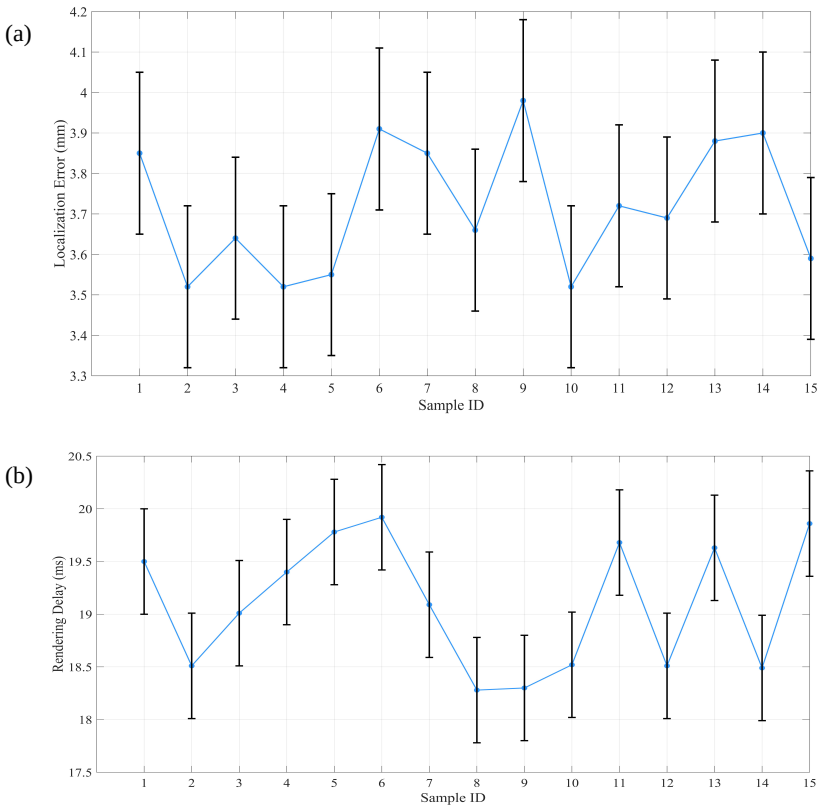

Figure 7. AR system performance evaluation. Figure 7 (a) Positioning error; Figure 7 (b) Rendering delay.

Figure 7 is an AR system performance evaluation, Figure 7 (a) and (b) represent positioning error and rendering delay respectively. Figure 7 (a) shows the average error value and ±0.2 mm fluctuation range for each student. The values are concentrated between 3.5 and 4.0 mm, showing good consistency between virtual and real space. Figure 7 (b) shows the response time of the system under different students. The delay value is distributed between 18 and 20 ms, with an error bar of ±0.5 ms. This reflects that the system has high real-time and stability, and reflects the high-precision registration capability and efficient rendering performance of the AR module in the power substation training scenario.

The model improves its robustness in complex environments such as lighting changes and occlusions through feature extraction, 3D map matching, and IMU sensor data fusion, thereby achieving sub-millimeter

positioning accuracy. At the same time, at the rendering level, the system uses lightweight 3D modeling and efficient GPU acceleration strategies to ensure low latency characteristics of screen updates. This verifies the technical feasibility and practicality of the AR interaction model proposed in this paper in the application of power substation personnel training, and also provides a solid foundation for the real-time collaboration of the subsequent neuromorphic feedback module.

H. Hierarchical Evaluation of Scenario Complexity

The state-action space is constructed through the student's historical training data, and the task complexity factor is calculated by combining the response time and error rate. Different fault types are divided into three levels of complexity: low, medium, and high. Assume that the average response time of task k is $\mu(t_k)$, and its average error rate is ε_k. The complexity factor C_k is defined as the product of the two:

$$C_k = \mu(t_k) \cdot \varepsilon_k \quad (34)$$

According to the C_k value, tasks are divided into the following three complexity levels: low complexity: $C_k < 2.0$; medium complexity: $2.0 < C_k < 5.0$; high complexity: $C_k \geq 5.0$.

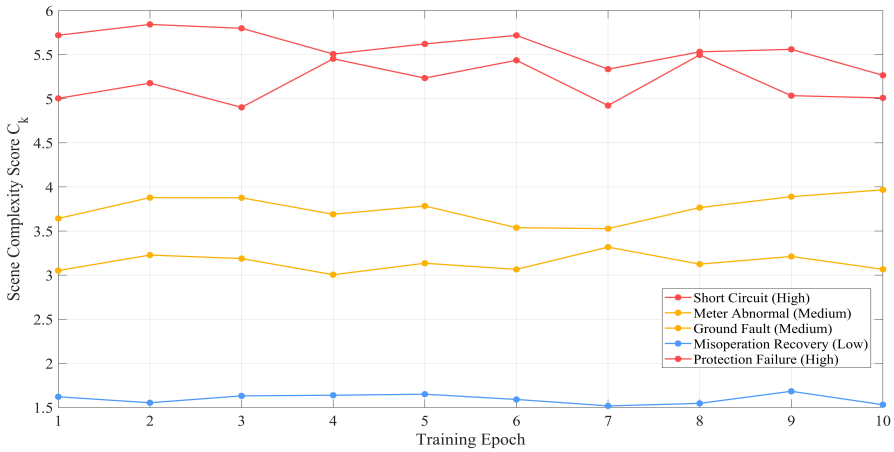

Figure 8. Layered evaluation of scenario complexity.

The horizontal axis in Figure 8 represents the training rounds (1 to 10 rounds), and the vertical axis represents the task complexity score C_k. The higher the value, the more complex the task requires of the trainee; each broken line represents a typical fault task, such as short-circuit tripping, protection malfunction, instrument abnormality, etc. Judging from the data, the short-circuit tripping and protection malfunction tasks always maintain a high complexity throughout the training process (average values are 5.6 and 5.2, respectively), and are classified as high complexity tasks. The error operation recovery task is stable at around 1.6, which is a low complexity task. Other tasks such as instrument abnormalities and grounding failure are between the two and constitute a medium complexity level. The complexity model constructed based on the product of response time and error rate enables the system to dynamically identify task difficulty and adjust teaching content.

The system uses Markov decision process modeling, combined with deep Q network strategy optimization, to dynamically update the state transition probability and reward function based on the student's historical training data to achieve a quantitative assessment of task complexity. High-complexity tasks such as short-circuit tripping have long response times and high error rates because they involve multiple devices linked to each other and real-time judgment, so they are rated high; while basic operation tasks such as error recovery processes are clear and have low error rates, so they are rated low. The system divides tasks into three categories, and matches tasks of corresponding levels to students with different mastery levels through multi-scenario knowledge transfer algorithms and adaptive generation mechanisms, achieving personalized teaching goals.

I. Long-term Effect Tracking

This paper conducts periodic retests on 15 students in the experimental group at 1, 2, 4, 6, and 8 weeks after completing all training, records their operation accuracy and task completion efficiency, and analyzes knowledge retention and skill transfer capabilities.

In each retest, trainees need to independently complete two types of tasks: standard operating procedures and emergency troubleshooting drills. The operation accuracy retention rate is defined as:

$$R_{\text{acc}}(t) = \frac{A(t)}{A_0} \quad (35)$$

A_0 is the operation accuracy at the end of training, and $A(t)$ is the average accuracy at the retest in week t. The task completion efficiency retention rate is defined as:

$$R_{\text{eff}}(t) = \frac{E(t)}{E_0} \quad (36)$$

E_0 is the task completion efficiency at the end of training, and $E(t)$ is the average completion efficiency at the retest in week t. The exponential decay model is used to fit the long-term memory retention curve:

$$R(t) = e^{-\lambda t} \quad (37)$$

λ is the forgetting rate coefficient, which reflects the tendency of knowledge or skills to decay over time.

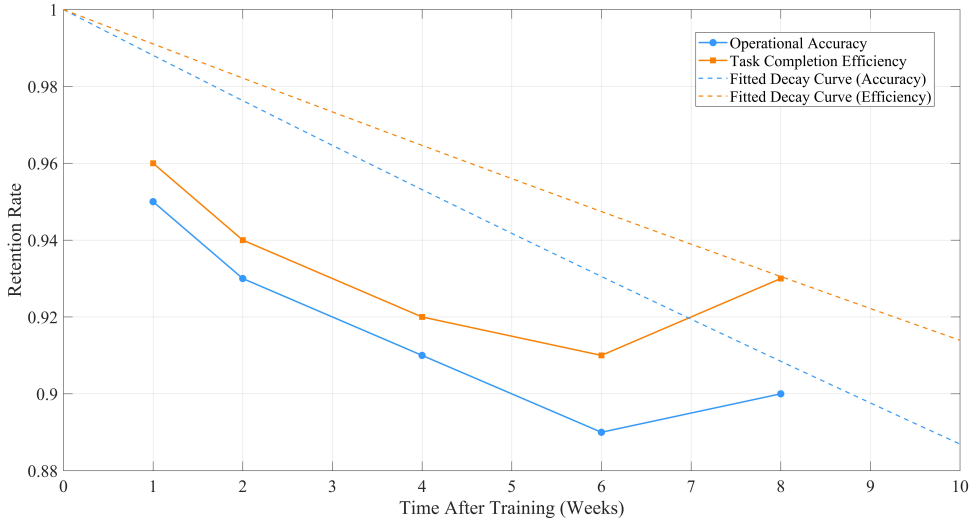

Figure 9. Long-term effect tracking.

Figure 9 shows the changing trends of the operation accuracy and task completion efficiency retention rate of the teaching system integrating AR and neuromorphic technology in the 1st, 2nd, 4th, 6th, and 8th weeks after the trainees completed the training, and fits the data with the exponential decay model. The horizontal axis is time; the vertical axis is retention rate. The measured points are represented by circles and squares to indicate the maintenance of operation accuracy and task completion efficiency, respectively, and the dotted line represents the fitted forgetting curve. At the 8th week, the maintenance rates of the operation accuracy and task completion efficiency of the experimental group students were 91% and 93%, respectively, indicating that the proposed teaching system has significant advantages in improving the persistence of students' skill mastery.

The SNN behavior recognition module improves the accuracy and timeliness of misoperation recognition by time-coding and pulse modeling the trainees' action trajectories, allowing trainees to form more stable action memories during training. AR guidance information and neuromorphic feedback mechanisms form a closed-loop teaching system, which enhances the ability to make immediate corrections and the effect of knowledge internalization during the learning process. At the same time, the multi-scenario adaptive generation mechanism dynamically adjusts the training difficulty according to the trainees' mastery status, so that trainees at different levels can continue to consolidate their knowledge structure at an appropriate challenge level. These mechanisms jointly support the high retention rate of learning outcomes and verify the feasibility and effectiveness of the proposed method in achieving the transformation from short-term reinforcement to long-term capacity building in power substation personnel training.

4. Statistical Analysis

Table 3 show that the experimental group is significantly better than the control group in all key indicators. The operation accuracy of the experimental group (87.6% ± 2.9) is significantly higher than that of the control group (75.0% ± 3.2), and the difference is highly statistically significant ($t = 5.23$, $p < 0.001$). The effect size (1.89) shows that this teaching method has a substantial impact on improving the operational standardization of trainees. In terms of emergency response efficiency, the average response time of the experimental group (57.8 s ± 3.1) is significantly shorter than that of the control group (73.4 s ± 4.5), and the statistical test also reaches a significant level ($t = 6.12$, $p < 0.001$). The effect size is as high as 2.15, indicating that the teaching system combining AR and neuromorphic technology can effectively shorten the trainees' response time to sudden failures and improve their emergency handling capabilities. The task completion rate of the experimental group (88.9% ± 3.7) was also significantly better than that of the control group (66.3% ± 4.1) ($t = 7.45$, $p < 0.001$, effect size = 2.58), reflecting the outstanding advantages of this method in multi-scenario adaptability and personalized teaching. In terms of knowledge mastery improvement, the difference between the pre-test and post-test scores of the experimental group (17.5 ± 2.8) was much higher than that of the control group (7.8 points ± 2.1) ($t = 5.98$, $p < 0.001$, effect size = 2.12), indicating that the

teaching system is effective in promoting knowledge internalization and long-term memory formation. The subjective immersion score results showed that the experimental group (4.7 ± 0.3) and the control group generally scored lower (3.2 ± 0.4), further verifying the positive role of AR and neuromorphic feedback mechanism in enhancing learning experience and improving participation. In summary, the intelligent teaching system based on AR and neuromorphic technology has shown significant advantages over traditional training methods in multiple dimensions and has good application prospects and promotion value.

Table 3. Comparison of Key Performance Indicators.

Metric	Control Group (n =15)	Experimental Group (n =15)	T -value	P -value	Effect Size
Operation Accuracy (%)	75.0 ± 3.2	87.6 ± 2.9	5.23	< 0.001	1.89
Emergency Response Time (s)	73.4 ± 4.5	57.8 ± 3.1	6.12	< 0.001	2.15
Task Completion Rate (%)	66.3 ± 4.1	88.9 ± 3.7	7.45	< 0.001	2.58
Knowledge Mastery Improvement (points)	7.8 ± 2.1	17.5 ± 2.8	5.98	< 0.001	2.12
Subjective Immersion Score (points)	3.2 ± 0.4	4.7 ± 0.3	8.56	< 0.001	2.92

5. Conclusions

This paper combines AR and neuromorphic technology to propose a multi-scenario fusion teaching optimization method for power substation personnel training. By building an AR interactive model based on SLAM to realize virtual-reality fusion operation guidance, this paper designs an SNN behavior recognition module for temporal action modeling, and introduces multi-scenario knowledge transfer and adaptive generation mechanisms, which effectively improves the students' operational standardization, emergency response efficiency and knowledge mastery under complex working conditions. The experimental results show that this method significantly improves the average operation accuracy and average task completion efficiency of trainees, and the operation accuracy and task completion efficiency retention rates of trainees after 8 weeks of training reach 91% and 93% respectively, enhancing the immersiveness of training and the ability to adapt teaching to personalization. The AR system also has high real-time and stability (positioning errors are mainly concentrated in 3.5~4.0 mm; rendering delays are mainly concentrated in 18~20 ms). In the future, edge computing and brain-computer interface technologies can be further integrated to promote the development of intelligent training systems towards higher levels of human-like cognitive capabilities, providing more efficient technical support for the cultivation of intelligent talents in the power industry.

Consent to Publish

The manuscript has not been published before, and it is not being reviewed by any other journal. The authors have all approved the content of the paper.

Funding

This work was supported by Science and Technology Project of State Grid Shanxi Electric Power Company, Lvliang Power Supply Company(5205J0240002).

Data Availability Statement

The data that support the findings of this study are available from the corresponding author, upon request.

Conflicts of Interest

The authors affirm that they do not have any financial conflicts of interest.

References

[1] L.J. Ge, Y.L. Li, Y.L. Li, J. Yan, Y.H. Sun. Smart distribution network situation awareness for high-quality operation and maintenance: a brief review. Energies, 2022, 15(3), 828. DOI: 10.3390/en15030828

[2] N.K. Mahato, J.X. Yang, J.F. Yang, G.J. Gong, J.H. Hao. Physical Security Auditing for Utilities: A Guide to Resilient Substation. Safety, 2024, 10(3), 80. DOI: 10.3390/safety10030080

[3] J. Gaspar, T. Cruz, C.T. Lam, P. Simoes. Smart substation communications and cybersecurity: A comprehensive survey. IEEE Communications Surveys & Tutorials, 2023, 25(4), 2456-2493. DOI: 10.1109/COMST.2023.3305468

[4] B.L. Li, Y.F. Ma, C. Zhang, F.W. Chu, Y.R. Chen, P. Quan. Research and application of digital electrical substation virtual engineering education system. Computer Applications in Engineering Education, 2024, 32(6), e22777. DOI: 10.1002/cae.22777

[5] H.J. Seo, G.M. Park, M.J. Son, A.J. Hong. Establishment of virtual-reality-based safety education and training system for safety engagement. Education Sciences, 2021, 11(12), 786. DOI: 10.3390/educsci11120786

[6] Y.J. Yan, Y.D. Liu, J. Fang, Y.F. Lu, X.C. Jiang. Application status and development trends for intelligent perception of distribution network. High Voltage, 2021, 6(6), 938-954. DOI: 10.1049/hve2.12159

[7] M. Perez-Ramirez, G. Arroyo-Figueroa, A. Ayala. The use of a virtual reality training system to improve technical skill in the maintenance of live-line power distribution networks. Interactive Learning Environments, 2021, 29(4), 527-544. DOI: 10.1080/10494820.2019.1587636

[8] T. Xue, C.D. Wu. Target detection of substation electrical equipment from infrared images using an improved faster regions with convolutional neural network features

algorithm. Insight-Non-Destructive Testing and Condition Monitoring, 2023, 65(8), 423-432. DOI: 10.1784/insi.2023.65.8.423

[9] G. Singh, A. Mantri, O. Sharma, R. Kaur. Virtual reality learning environment for enhancing electronics engineering laboratory experience. Computer Applications in Engineering Education, 2021, 29(1), 229-243. DOI: 10.1002/cae.22333

[10] I.F. Mondragón Bernal, N.E. Lozano-Ramírez, J.M. Puerto Cortés, S. Valdivia, R. Munoz, J. Aragon, et al. An immersive virtual reality training game for power substations evaluated in terms of usability and engagement. Applied Sciences, 2022, 12(2), 711. DOI: 10.3390/app12020711

[11] T. Yang, Y.C. Hou, Y.C. Liu, F. Zhai, R.Z. Niu. WPD-ResNeSt: Substation station level network anomaly traffic detection based on deep transfer learning. CSEE Journal of Power and Energy Systems, 2021, 10(6), 2610-2620. DOI: 10.17775/CSEEJPES.2020.02850

[12] J.H. Ou, J.G. Wang, J. Xue, J.P. Wang, X. Zhou, L.C. She. Infrared image target detection of substation electrical equipment using an improved faster R-CNN. IEEE Transactions on Power Delivery, 2022, 38(1), 387-396. DOI: 10.1109/TPWRD.2022.3191694

[13] E.A. Felinska, T.E. Fuchs, A. Kogkas, Z.W. Chen, B. Otto, K.F. Kowalewski, et al. Telestration with augmented reality improves surgical performance through gaze guidance. Surgical Endoscopy, 2023, 37(5), 3557-3566. DOI: 10.1007/s00464-022-09859-7

[14] Y. Ke, H.T. Chen, Z.Y. Liu, Z.Y. Yang. Perception and early warning technology of power substation safety construction operation based on multi-dimensional information fusion. International Journal of Wireless and Mobile Computing, 2024, 26(4), 408-415. DOI: 10.1504/IJWMC.2024.138856

[15] J. Song, J. Kook. Visual SLAM based spatial recognition and visualization method for mobile AR systems. Applied System Innovation, 2022, 5(1), 11. DOI: 10.3390/asi5010011

[16] V. Sadhu, K. Anjum, D. Pompili. On-board deep-learning-based unmanned aerial vehicle fault cause detection and classification via fpgas. IEEE Transactions on Robotics, 2023, 39(4), 3319-3331. DOI: 10.1109/TRO.2023.3269380

[17] H.L. Liu, F.Q. Gu, Z.X. Lin. Auto-sharing parameters for transfer learning based on multi-objective optimization. Integrated Computer-Aided Engineering, 2021, 28(3), 295-307. DOI: 10.3233/ICA-210655

[18] Y.X. Zhao, Z. Cen. Exploring Multimodal Feedback Mechanisms for Improving User Interaction in Virtual Reality Environments. Journal of Industrial Engineering and Applied Science, 2024, 2(6), 35-41. DOI: 10.70393/6a69656173.323331

[19] Y.J. Li, X.W. Wang, F.K. Chen, B.X. Zhao, Q. Fu. Online Learning Behavior Analysis and Prediction Based on Spiking Neural Networks. Journal of Social Computing, 2024, 5(2), 180-193. DOI: 10.23919/JSC.2024.0015

[20] G. Marchesi, C. Eichhorn, D.A. Plecher, Y. Itoh, G. Klinker. Envslam: Combining slam systems and neural networks to improve the environment fusion in ar applications. ISPRS International Journal of Geo-Information, 2021, 10(11), 772. DOI: 10.3390/ijgi10110772

[21] K. Minoda, F. Schilling, V. Wüest, D. Floreano, T. Yairi. Viode: A simulated dataset to address the challenges of visual-inertial odometry in dynamic environments. IEEE Robotics and Automation Letters, 2021, 6(2), 1343-1350. DOI: 10.1109/LRA.2021.3058073

[22] H.L. Li, J. Stueckler. Visual-inertial odometry with online calibration of velocity-control based kinematic motion models. IEEE Robotics and Automation Letters, 2022, 7(3), 6415-6422. DOI: 10.1109/LRA.2022.3169837

[23] L.Y. Niu, Y. Wei, W.B. Liu, J.Y. Long. Research Progress of spiking neural network in image classification: a review. Applied Intelligence, 2023, 53(16), 1-25. DOI: 10.1007/s10489-023-04553-0

[24] N. Rathi, K. Roy. Diet-snn: A low-latency spiking neural network with direct input encoding and leakage and threshold optimization. IEEE Transactions on Neural Networks and Learning Systems, 2021, 34(6), 3174-3182. DOI: 10.1109/TNNLS.2021.3111897

[25] X.B. Jin, M. Zhang, R. Yan, G. Pan, D. Ma. R-SNN: Region-based spiking neural network for object detection. IEEE Transactions on Cognitive and Developmental Systems, 2023, 16(3), 810-817. DOI: 10.1109/TCDS.2023.3311634

[26] I. Spinelli, S. Scardapane, A. Uncini. A meta-learning approach for training explainable graph neural networks. IEEE Transactions on Neural Networks and Learning Systems, 2022, 35(4), 4647-4655. DOI: 10.1109/TNLS.2022.3171398

[27] V.C. Luu, J.P. Hong. GNN-based meta-learning approach for adaptive power control in dynamic D2D communications. IEEE Transactions on Vehicular Technology, 2023, 73(4), 1-6. DOI: 10.1109/TVT.2023.3332809

[28] I. Nikoloska, O. Simeone. Modular meta-learning for power control via random edge graph neural networks. IEEE Transactions on Wireless Communications, 2022, 22(1), 457-470. DOI: 10.1109/TWC.2022.3195352

[29] J. You, Z.Y. Wu, W. Wei, N. Li, Y.H. Yang. Evolution of Industrial Robots from the Perspective of the Metaverse: Integration of Virtual and Physical Realities and Human–Robot Collaboration. Applied Sciences, 2024, 14(14), 6369. DOI: 10.3390/app14146369

[30] N.Z. Qiao, L. Dong, C.Y. Sun. Adaptive deep learning network with multi-scale and multi-dimensional features for underwater image enhancement. IEEE Transactions on Broadcasting, 2022, 69(2), 482-494. DOI: 10.1109/TBC.2022.3227424